# Structural changes in the myosin filament and cross-bridges during active force development in single intact frog muscle fibres: stiffness and X-ray diffraction measurements

E. Brunello[1,2], P. Bianco[1,2], G. Piazzesi[1,2], M. Linari[1], M. Reconditi[1], P. Panine[3], T. Narayanan[3], W.I. Helsby[4], M. Irving[5] and V. Lombardi[1,2]

[1]*Laboratory of Physiology, Department of Animal Biology and Genetics, University Florence, Via G. Sansone 1, 50019 Sesto Fiorentino, Italy*
[2]*Centro di Ricerca e Sviluppo SOFT-INFM-CNR, Università di Roma 'La Sapienza' , Italy*
[3]*European Synchrotron Radiation Facility, Grenoble, France*
[4]*Council for the Central Laboratory of the Research Councils, Daresbury, UK*
[5]*Randall Division of Cell and Molecular Biophysics, King's College London, London SE1 1UL, UK*

**Structural and mechanical changes occurring in the myosin filament and myosin head domains during the development of the isometric tetanus have been investigated in intact frog muscle fibres at 4°C and 2.15 $\mu$m sarcomere length, using sarcomere level mechanics and X-ray diffraction at beamline ID2 of the European Synchrotron Radiation Facility (Grenoble, France). The time courses of changes in both the M3 and M6 myosin-based reflections were recorded with 5 ms frames using the gas-filled RAPID detector (MicroGap Technology). Following the end of the latent period (11 ms after the start of stimulation), force increases to the tetanus plateau value ($T_0$) with a half-time of 40 ms, and the spacings of the M3 and M6 reflections ($S_{M3}$ and $S_{M6}$) increase by 1.5% from their resting values, with time courses that lead that of force by ∼10 and ∼20 ms, respectively. These temporal relations are maintained when the increase of force is delayed by ∼10 ms by imposing, from 5 ms after the first stimulus, 50 nm (half-sarcomere)$^{-1}$ shortening at the velocity ($V_0$) that maintains zero force. Shortening at $V_0$ transiently reduces $S_{M3}$ following the latent period and delays the subsequent increase in $S_{M3}$, but only delays the $S_{M6}$ increase without a transient decrease. Shortening at $V_0$ imposed at the tetanus plateau causes an abrupt reduction of the intensity of the M3 reflection ($I_{M3}$), whereas the intensity of the M6 reflection ($I_{M6}$) is only slightly reduced. The changes in half-sarcomere stiffness indicate that the isometric force at each time point is proportional to the number of myosin heads bound to actin. The different sensitivities of the intensity and spacing of the M3 and M6 reflections to the mechanical responses support the view that the M3 reflection in active muscle originates mainly from the myosin heads attached to the actin filament and the M6 reflection originates mainly from a fixed structure in the myosin filament signalling myosin filament length changes during the tetanus rise.**

(Received 14 June 2006; accepted after revision 19 September 2006; first published online 21 September 2006)
**Corresponding author** V. Lombardi: Laboratory of Physiology, Department of Animal Biology and Genetics, University Florence, Via G. Sansone 1, 50019 Sesto Fiorentino, Italy. Email: vincenzo.lombardi@unifi.it

In skeletal muscle the development of force during isometric contraction is due to the globular myosin heads, emerging from the myosin filament, that attach to the actin filament and undergo a structural change that increases the strain in the myofilaments and attached myosin heads themselves. This process can be investigated in intact muscle cells using time-resolved X-ray diffraction from whole muscle or single muscle fibres (Haselgrove & Huxley, 1973; Huxley *et al.* 1982; Cecchi *et al.* 1991; Martin-Fernandez *et al.* 1994). These studies indicated that the development of the force in an isometric tetanus follows the radial and azimuthal movements of the myosin heads with a significant delay. The temporal lead of the increase of muscle fibre stiffness over that of force suggested that there is a slow step between attachment of myosin heads to actin and force generation (Cecchi *et al.* 1982; Ford *et al.* 1986). However, the discovery that at least half of the compliance of the muscle sarcomere

 DOI: 10.1113/jphysiol.2006.115394

resides in the actin and myosin filaments (Huxley *et al.* 1994; Wakabayashi *et al.* 1994) raised the possibility of an alternative explanation for the delay between the rise of sarcomere stiffness and force.

X-ray diffraction studies of isometrically contracting muscle show that the myosin-based reflections, apart from the third- (M3) and sixth-order (M6) reflections on the meridional axis (parallel to the fibre axis), undergo an early drop in intensity following tetanic stimulation, as a consequence of the loss of the quasi-helical order of the resting myosin filament (Huxley *et al.* 1982). The spacings of the M3 and M6 reflections ($S_{M3}$ and $S_{M6}$, respectively) increase on activation; $S_{M3}$ increases from 14.34 nm at rest to 14.56 nm at the tetanus plateau (force $= I_o$), and $S_{M6}$ increases from 7.16 nm at rest to 7.28 nm at the tetanus plateau (Huxley & Brown, 1967; Huxley *et al.* 1982; Bordas *et al.* 1993; Linari *et al.* 2000). These changes lead the rise of isometric force and are one order of magnitude larger than those expected from the instantaneous elasticity of the myosin filament, $\sim 0.26\%/T_0$ (Huxley *et al.* 1994; Wakabayashi *et al.* 1994; Reconditi *et al.* 2004; Linari *et al.* 2005). Therefore they cannot be simply related to the increase in the stress on the filament, and their underlying mechanism is still unclear.

Another open question is whether the M3 and M6 reflections originate from different structures in the myosin filament (Huxley *et al.* 2003). The fine structure of the M3 and M6 reflections can be explained by attributing both reflections to the myosin heads only if the partner detached head of the same myosin molecule is displaced axially by $\sim$7 nm with respect to the attached head, and the conformational disorder of both is less than $\sim$1 nm (Juanhuix *et al.* 2001). On the other hand, much evidence indicates that, in active muscle, the M3 but not the M6 reflection originates mainly from the attached myosin heads. Both the intensity and fine structure of the M3 reflection are sensitive to fast perturbations in length or load that induce axial movements of the myosin heads (Piazzesi *et al.* 2002; Reconditi *et al.* 2004). In contrast, the M6 reflection is much less sensitive to fast mechanical manoeuvres, and should therefore originate from a fixed structure in the myosin filament. The low contribution of the myosin heads to the M6 reflection during isometric contraction can be explained if the attached heads have significant axial dispersion (Reconditi *et al.* 2004).

In this work, we report the structural and mechanical changes undergone by the myosin filament and myosin heads during the development of the isometric tetanus. We determined the time courses of both the intensity and spacing of the M3 and M6 reflections, and the stiffness of a selected population of sarcomeres monitored with a striation follower (Huxley *et al.* 1981). To discriminate the effects of activation from those of force generation, ramp shortening of $\sim$50 nm (half-sarcomere)$^{-1}$ was imposed during the tetanus rise at a velocity sufficient to maintain the force at the value just before the start of shortening. The results show that the increase in isometric force follows very rapidly the attachment of myosin heads to actin and that the structural change in the myosin filament during activation can be delayed by holding the force at zero. The M3 and M6 reflections have different sensitivities to this mechanical manoeuvre, and this is consistent with their different structural origins.

## Methods

### Preparation and mounting of the muscle fibres

The experiments were performed at beamline ID2 of the European Synchrotron Radiation Facility (ESRF). Frogs (*Rana temporaria*) were killed by decapitation followed by destruction of the brain and the spinal cord according to the official regulation of the European Community Council, Directive 86/609/EEC and conforming with the UK Animals Scientific Procedures Act, 1986. Single fibres (5–6.5 mm long) were dissected from the tibialis anterior muscle and mounted horizontally in a trough with Ringer solution between a capacitance force transducer (Huxley & Lombardi, 1980) and a loudspeaker coil motor (Lombardi & Piazzesi, 1990). The ringer solution composition was (mM): NaCl 115, KCl 2.5, $CaCl_2$ 1.8, phosphate buffer 3 (pH 7.1). Two mica windows were moved close to the fibre to reduce the X-ray path in Ringer solution to 300 $\mu$m on each side of the fibre. Trains of stimuli of alternate polarity were delivered by means of platinum wire electrodes stuck on the top and bottom edges of the opposing windows to elicit fused tetani. Sarcomere length, fibre length and cross-sectional area were measured under a microscope with a $\times$40 water immersion objective and a $\times$25 eyepiece. A striation follower (Huxley *et al.* 1981) was used to record the length of a population of sarcomeres in a 1–2 mm segment of the fibre selected close to the force transducer end to minimize the effect of the propagation time of mechanical perturbations.

### X-ray data collection

The ID2 beamline provided an X-ray flux of up to $3 \times 10^{13}$ photons s$^{-1}$ at 0.1 nm wavelength. Diffraction patterns from a muscle fibre were collected with 5 ms exposure time on two-dimensional detectors of area $200 \times 200$ mm$^2$, mounted 3–3.5 m from the fibre to include the sixth-order myosin meridional reflection (M6). The detector was either gas-filled (RAPID, MicroGap Technology (Lewis *et al.* 1992)), temporarily installed at the beamline, or a CCD-based detector with image intensifier (FReLoN (Narayanan *et al.* 2001)). A fast electromagnetic shutter (LS500, nmLaser Products, Inc., Sunnyvale, CA, USA; switching time, 40 $\mu$s) in front of the fibre ensured that it was exposed to X-rays only during the data collection period, to minimize radiation damage.

The RAPID detector allowed a complete sequence of 5 ms time frames to be collected in a single tetanus, providing an estimate of the time course of the changes of the intensity of the reflections more reliably than with the CCD detector, which requires that different time frames are collected in different tetani. However the RAPID detector has a lower efficiency for X-rays of wavelength 0.1 nm, and the signal to noise ratio was too low for a reliable analysis of individual 5 ms time frames. The signal to noise ratio was increased by adding corresponding time frames from many tetani and from different fibres. To achieve a better signal to noise ratio for the weaker M6 reflection, experiments were repeated in a subsequent visit to the beamline using the FReLoN detector. Before the read-out of the CCD, its 2048 × 2048 pixels were binned by 16 in the radial direction and 2 in the axial direction to increase the signal to noise ratio and to allow consecutive time frames to be read out with a minimum interval of 35 ms. Two frames were collected in each tetanus, and 14 tetani were necessary to describe the complete rising phase of the tetanus.

### Experimental protocol

Tetanic contractions of 360 ms duration were induced every 4 min at 4°C and at ∼2.15 $\mu$m sarcomere length by electrical stimulation at a frequency of 15–25 Hz. The development of isometric tension was in fixed-end mode (rather than in sarcomere length-clamp mode) to minimize the possibility that X-ray data collected in subsequent tetani could be affected by artefacts generated by an unpredictable deterioration of the sarcomere length signal. Particular care was taken to minimize the compliance of the tendon attachments, and only fibres with less than 25 nm (half-sarcomere)$^{-1}$ shortening during the rise of the tetanus were used for either mechanical or X-ray measurements.

Ramp shortening of 50 nm (half-sarcomere)$^{-1}$ was imposed on the fibre during the tetanus rise at the velocity required to maintain the force at the value just before the start of shortening. Each tetanus with shortening during force development was followed by one with the same shortening ramp imposed at the tetanus plateau.

Changes in stiffness of the half-sarcomere during the tetanus rise were determined in separate experiments by imposing small (2 nm (half-sarcomere)$^{-1}$ peak-to-peak), 4 kHz sinusoidal length changes at one fibre end and measuring the change in half-sarcomere length from a fibre segment selected near the other end, which was connected to the force transducer. In this way, the propagation delay between the length and force signals was minimized, and there was no significant contribution of out-of-phase stiffness, even at low force during the tetanus rise. Oscillations were imposed either at the plateau of the isometric tetanus ($T_0$) or at 0.25 $T_0$, 0.5 $T_0$ and 0.75 $T_0$ during the tetanus rise. The number of cycles of the oscillation ranged from 10 to 20. The number was adjusted according to the rate of force development so that the force increase from the beginning to the end of the oscillations never exceeded 0.07 $T_0$.

### Data analysis

X-ray diffraction patterns were analysed using the SAXS package (P. Boesecke, ESRF), Fit2D (A. Hammersley, ESRF), Peakfit software (SPSS Science) and IgorPro (WaveMetrics, Inc.).

Images were centred and aligned using the M3 reflections on the two sides of the pattern. The distribution of diffracted intensity along the meridional axis of the X-ray pattern (parallel to the fibre axis) was calculated by integrating from 0.013 nm$^{-1}$ on either side of the axis. The background intensity distribution was fitted using a convex hull algorithm and subtracted. The intensity profile of each reflection was fitted with a Gaussian function, so that the total intensity and spacing were determined as the area and centre of the Gaussian, respectively. Axial spacings were calibrated using the spacing of the M3 reflection in the resting fibre (Haselgrove, 1975) (14.34 nm). The cross-meridional width of the reflections (perpendicular to the fibre axis) was determined by measuring the full width at half-maximum of the intensity distribution obtained by integrating along the meridional axis. Integration limits were 0.062–0.078 nm$^{-1}$ for the M3 reflection and 0.131–0.147 nm$^{-1}$ for the M6 reflection. The full width at half-maximum of the beam was about 500 $\mu$m and the point spread function of the RAPID detector was about 400 $\mu$m. The combined instrumental point spread function was 5 and 20 times smaller than the radial width of the M3 reflection at rest and the tetanus plateau, respectively, so the radial width of the reflection was not corrected for the instrumental point spread function.

The time courses of the parameters of X-ray reflections during the tetanus rise were analysed by fitting a sigmoid curve and determining the time to half-maximum ($t_{1/2}$) of the change from the resting to the plateau value. Except where noted otherwise, the time to half-maximum of both the force and the structural signals was measured from the end of the latent period in the isometric tetanus, which occurs at a time $t_s$ after the first stimulus (Haugen & Sten-Knudsen, 1976). The time course of the isometric force rise was estimated by the average of the times to half-maximum force from each fibre.

Mechanical parameters (force, stimulus frequency, fibre length change and sarcomere length change) and X-ray framing were collected and analysed with LabVIEW (National Instruments Co, Austin, TX, USA) software. The elastic and viscous components of the complex stiffness were calculated by Fourier analysis of the force and length

signals. Viscous stiffness was never larger than 1% of elastic stiffness.

## Results

### Time course of fibre stiffness during the development of the isometric force

Following electrical stimulation, the force (upper line in Fig. 1*A*) starts to rise at the end of the latent period ($t_s$) at $11.5 \pm 0.6$ ms (mean ± s.d., $n = 4$ fibres) after the first stimulus and attains its plateau value ($T_0$) with a half-time, measured from $t_s$, of $39.4 \pm 5.5$ ms. The sarcomere shortening during the force rise (lower line in Fig. 1*A*) was $23.8 \pm 11.8$ nm (half-sarcomere)$^{-1}$. Small (∼2 nm peak-to-peak) sinusoidal length changes, composed of 10–20 cycles of 250 $\mu$s period (Fig. 1*B*), were superimposed at $37.3 \pm 2.2$, $55.8 \pm 4.3$, $78.8 \pm 6.0$ and $282.0 \pm 3.3$ ms after the start of stimulation, when the force was $0.26 \pm 0.02$ $T_0$, $0.52 \pm 0.02$ $T_0$, $0.78 \pm 0.05$ $T_0$ and $T_0$, respectively. Stiffness ($e$), estimated as the elastic modulus extracted by Fourier analysis from the force and sarcomere length oscillations, was $0.10 \pm 0.01$, $0.17 \pm 0.02$, $0.20 \pm 0.02$ and $0.23 \pm 0.02$ $T_0$ nm$^{-1}$ at 0.26 $T_0$, 0.52 $T_0$, 0.78 $T_0$, and $T_0$, respectively. When normalized by its value at the tetanus plateau ($e_0$), the increase in stiffness leads relative force throughout the rise of the isometric tetanus (Fig. 1*A*, filled circles). The ratio of stiffness to force is always greater than unity (Fig. 1*C*, filled circles) (Cecchi *et al.* 1982, 1987; Ford *et al.* 1986).

### Compliance of myofilaments and myosin cross-bridges

The lead of stiffness over force during the tetanus rise (Fig. 1*A*) may be due to the contribution of myofilaments

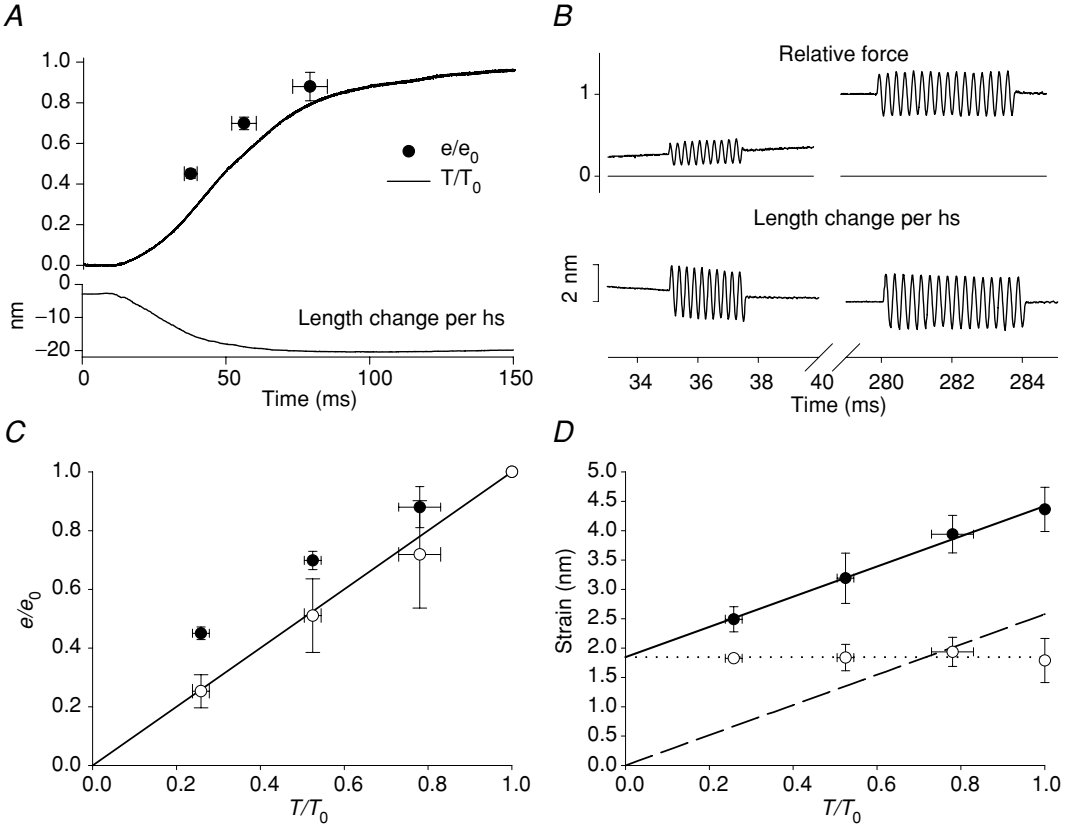


**Figure 1. Stiffness and strain of the half-sarcomere during the rise of the isometric tetanus**
*A*, time course of force ($T$, thick line), stiffness ($e$, ●) and half-sarcomere shortening (nm, thin line) during the tetanus rise. Force and stiffness are relative to the tetanic plateau values $T_0$ and $e_0$, respectively. Zero time is the start of stimulation. *B*, force (relative to $T_0$) and length change per half-sarcomere (nm) during 4 kHz sinusoidal length changes imposed 35 ms and 280 ms after the start of stimulation when force was 0.25 $T_0$ and $T_0$. *C*, half-sarcomere stiffness (●) and cross-bridge stiffness (○) plotted against the force developed during the tetanus rise. Cross-bridge stiffness is calculated from the open circles in *D* as explained in the text. The line represents the direct proportionality between stiffness and force. *D*, half-sarcomere strain (●) plotted against force; the slope of the straight line fitted to these points ($2.6 \pm 0.1$ nm $T_0^{-1}$) represents the filament strain (dashed line). Cross-bridge strain (○) obtained by subtracting filament strain from half-sarcomere strain. Dotted line is the linear regression of these data.

to the half-sarcomere compliance (Huxley *et al.* 1994; Wakabayashi *et al.* 1994). At any time during the tetanus rise the compliance of the half-sarcomere is the sum of a variable contribution from the myosin cross-bridges and a constant contribution from the myofilaments, which are effectively in series. The relationship between the half-sarcomere strain ($s_{hs}$; calculated as the ratio between force and stiffness of the half-sarcomere ($T/e$)) and the force at different times during the tetanus rise (Fig. 1*D*, filled circles) therefore provides an estimate of the relative strains of the two structures. Linear regression of this relationship gave a slope of $2.6 \pm 0.1$ nm $(T/T_0)^{-1}$ and an intercept on the ordinate of $1.8 \pm 0.1$ nm (mean ± s.D.). The slope is a compliance and can be expressed in standard units (nm kPa$^{-1}$) using the plateau force ($217 \pm 28$ kPa in these experiments). The resulting compliance, $0.012 \pm 0.002$ nm kPa$^{-1}$, is similar to the compliance of the actin and myosin filaments estimated from mechanical and X-ray structural experiments (Piazzesi *et al.* 2002; Reconditi *et al.* 2004; Decostre *et al.* 2005). The ordinate intercept, 1.8 nm, then represents the average strain of the array of the myosin heads attached in the half-sarcomere ($s_{cb}$ (Piazzesi *et al.* 2002; Reconditi *et al.* 2004; Decostre *et al.* 2005)). $s_{cb}$ (Fig. 1*D*, open circles) was calculated at each force by subtracting the filament compliance (dashed line in Fig. 1*D*) from the observed value of $s_{hs}$, and remains constant during the tetanus rise. The stiffness of attached myosin heads is given by $T/s_{cb}$, and increases in proportion to the force $T$ (Fig. 1*C*, open circles). Assuming that the stiffness of an individual myosin head is constant during the tetanus rise, the fraction of heads attached is given by $T/(s_{cb}\, k_b)$, where $k_b$ is the cross-bridge stiffness when all heads are attached. Thus during the rise of the isometric tetanus the force is proportional to the number of attached heads, and the force per attached head is constant.

### Time course of X-ray changes during the development of the isometric force and the effect of unloaded shortening

X-ray signals were recorded with 5 ms time frames both in tetanic contractions that started in isometric conditions (thick lines and filled symbols in Figs 2 and 3) and in tetanic

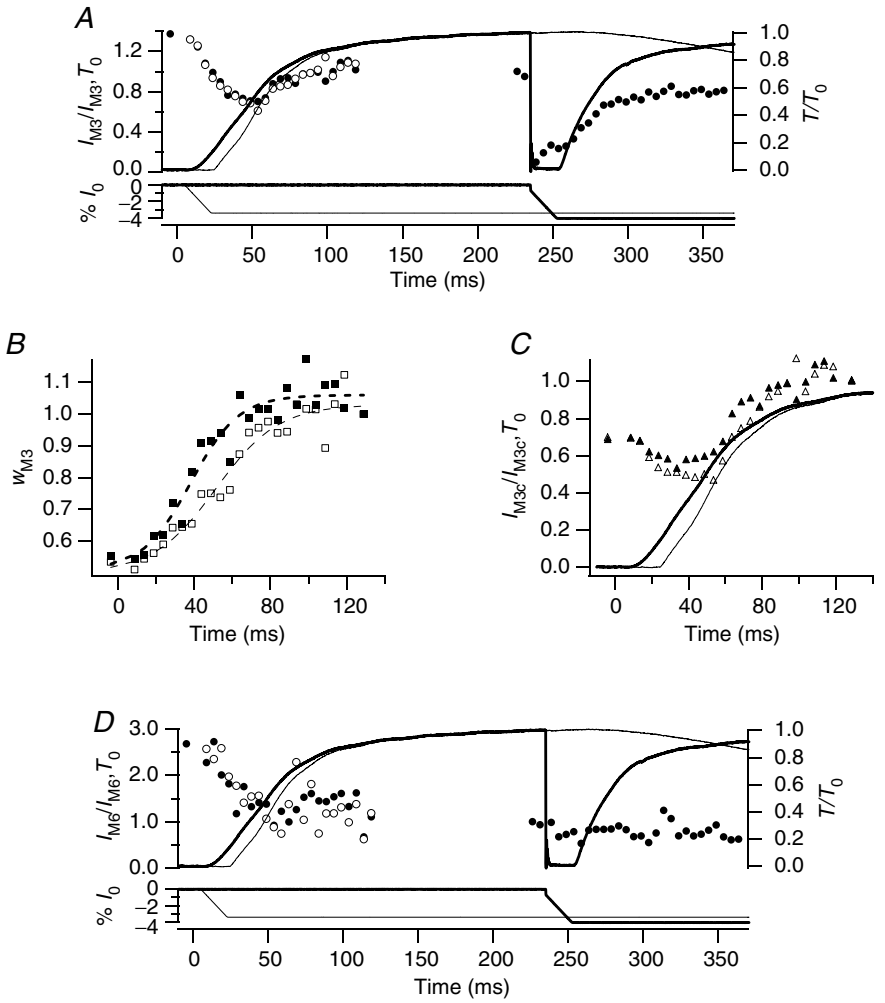


**Figure 2. X-ray intensity changes during the rise of the tetanus and during unloaded shortening**
In each panel filled symbols refer to X-ray data collected in tetani with the unloaded shortening imposed at the isometric plateau; open symbols refer to X-ray data collected in tetani with unloaded shortening imposed 5 ms after the start of stimulation. Data were collected on the RAPID detector with 5 ms time frames. Zero time is the start of stimulation. *A*, circles, intensity of M3 reflection ($I_{M3}$) relative to the plateau value; lines, force (relative to $T_0$, upper traces) and imposed length changes (% of fibre length ($l_0$), lower traces). Thick lines, tetanus with unloaded shortening imposed at the plateau; thin lines, unloaded shortening imposed at 5 ms after the start of stimulation. *B*, squares, cross-meridional width of the M3 reflection ($w_{M3}$), relative to the isometric plateau value, during tetanus rise. Dashed lines, sigmoid fits to the data. *C*, triangles, time course of $I_{M3}$ after width correction ($I_{M3c} = I_{M3} \times w_{M3}$). Continuous lines, force traces as in *A*. *D*, circles, intensity of M6 reflection ($I_{M6}$) relative to the plateau value; lines, force and length traces as in *A*.

contractions in which the initial force rise was delayed by imposing ramp shortening of ~50 nm (half-sarcomere)$^{-1}$ at the minimum velocity ($V_0$) that maintained the force of the active fibre at zero (thin lines and open symbols in Figs 2 and 3). In this group of fibres, $t_s$ was 11.4 ± 1.2 ms (mean ± S.D., $n = 8$ fibres) in isometric conditions. $V_0$ shortening started 5 ms after the first stimulus, roughly halfway through the latent period, and ended 29.8 ± 6.2 ms after the first stimulus. Relevant data from the eight fibres analysed are summarized in Table 1. The half-time for isometric force development, estimated as the time from $t_s$ to 0.5 $T_0$, was 41.4 ± 13.1 ms (Table 1*B*). In tetani with superimposed initial shortening, force started to develop at the end of the shortening with a time course that was slightly faster than that of the force rise in isometric conditions: the half-time, measured from the end of shortening, was 37.2 ± 14.8 ms.

To obtain a comparative estimate of the effects of unloaded shortening at full activation, the same ramp shortening was imposed at the plateau of an otherwise isometric tetanus (235 ms after the start of stimulation, Figs 2 and 3). In this case the ramp shortening was preceded by a step release (7–8 nm (half-sarcomere)$^{-1}$), to accelerate the drop of force to zero. The time course of force redevelopment following the end of unloaded shortening was faster than the initial isometric rise, mainly as a result of acceleration of the early force increase: the half-time of force redevelopment, measured from the end of the shortening, was 20.2 ± 2.4 ms.

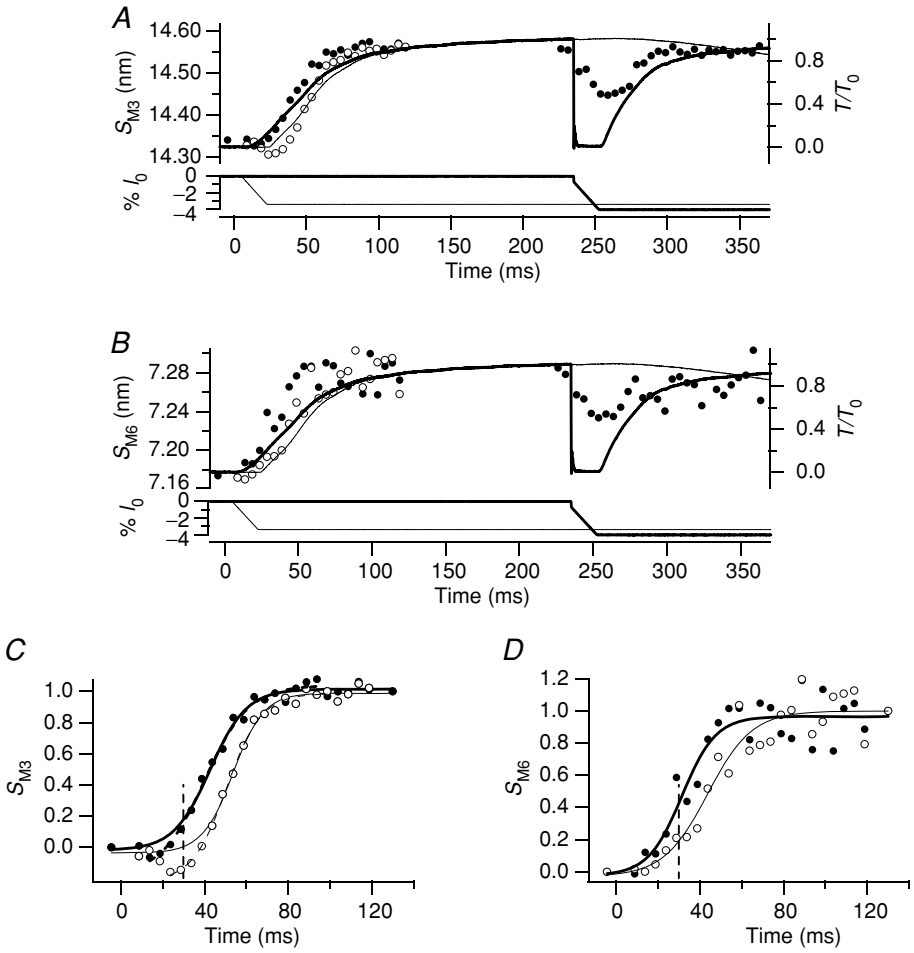


**Figure 3. Spacing changes during the tetanus rise and during unloaded shortening**
Same experiments as Fig. 2. *A* and *B*, spacings of M3 and M6 reflections, $S_{M3}$ and $S_{M6}$, respectively. Thick and thin lines, and filled and open circles according to the description in Fig. 2*A*. *C*. fractional change in $S_{M3}$ between rest and tetanus plateau. Continuous lines, sigmoid fits to data lying above 0; dashed lines, sigmoid fit to data starting from the lowest value. In the isometric tetanus (thick lines), the half-time for $S_{M3}$ is 31.3 ± 1.6 ms for the continuous line and 30.9 ± 1.4 ms for the dashed line. In the tetanus with initial shortening (thin lines), the half-time for $S_{M3}$ is 42.2 ± 1.4 ms for the continuous line and 42.2 ± 1.3 ms for the dashed line. The vertical dashed line marks the end of unloaded shortening. *D*, fractional change in $S_{M6}$ between rest and tetanus plateau. Continuous lines, sigmoid fit to data. Vertical dashed line, end of unloaded shortening.

**Table 1. Mechanical and structural parameters collected in experiments with the RAPID detector**

| *A* RAPID | Rest | $T_0$ | $V_{0,\text{start}}$ | $V_{0,T0}$ |
|---|---|---|---|---|
| $S_{M3}$ (nm) | 14.34 | 14.56 | 14.31 | 14.48 |
| $S_{M6}$ (nm) | 7.17 | 7.28 | 7.19 | 7.24 |
| $I_{M3}$ | 1.37 (0.6) | 1 | — | 0.23 |
| $I_{M6}$ | 2.68 (1.1) | 1 | — | 0.73 |
| $w_{M3}$ | 0.5 | 1 | — | — |
| $w_{M6}$ | 0.4 | 1 | — | — |

| *B* RAPID | $t_{1/2,\text{force}}$ (ms) | $t_{1/2,\text{wM3}}$ (ms) | $t_{1/2,\text{SM3}}$ (ms) | $t_{1/2,\text{SM6}}$ (ms) |
|---|---|---|---|---|
| Isometric | $41.4 \pm 13.1$ | $26.8 \pm 4.2$ | $31.3 \pm 1.6$ | $20.0 \pm 3.5$ |
| $V_{0,\text{start}}$ | $55.2 \pm 15.6$ | $40.0 \pm 4.2$ | $42.2 \pm 1.4$ | $32.3 \pm 3.5$ |
| Smoothed isometric | — | — | $30.9 \pm 1.4$ | $20.3 \pm 2.1$ |
| Smoothed $V_0$ | — | — | $42.2 \pm 1.3$ | $32.3 \pm 2.7$ |

*A*, spacing, intensity and cross-meridional width of M3 and M6 reflections at rest, at the isometric tetanus plateau ($T_0$) and during steady shortening at $V_0$ imposed either 5 ms after the start of stimulation ($V_{0,\text{start}}$) or at the tetanus plateau ($V_{0,T0}$). X-ray data from eight fibres; $V_{0,\text{start}}$ and $V_{0,T0}$ values are the average of the last two frames before the end of shortening. $V_0$ in these fibres was $1.65 \pm 0.30$ $\mu$m s$^{-1}$ (half-sarcomere)$^{-1}$. $I_{M3}$ and $I_{M6}$ values inside the brackets are intensity values corrected for the cross-meridional width. *B*, half-times of change in force ($t_{1/2,\text{force}}$), cross-meridional width of the M3 reflection ($t_{1/2,\text{wM3}}$), spacing of M3 ($t_{1/2,\text{SM3}}$) and spacing of M6 ($t_{1/2,\text{SM6}}$) in the isometric tetanus (first row) and in the tetanus with shortening at $V_0$ imposed 5 ms after the start of stimulation (second row). The third and fourth rows report the time course of M3 and M6 spacings after two time-frame smoothing. The half-time of force is the mean ± S.D. of $n = 8$ fibres. The error for width and the spacing is provided by the sigmoid fitting program.

**Intensity of the M3 and M6 reflections.** During the tetanus rise the intensity of the M3 reflection ($I_{M3}$; Fig. 2*A*, filled circles) showed a transient decrease followed by an increase which started half-way through the tetanus rise and followed the remaining time course of force development. The initial drop of $I_{M3}$ (Fig. 2*A*) has been attributed to reduction of the lateral coherence between filaments (Huxley *et al.* 1982). In these experiments, the cross-meridional width of the reflection ($w_{M3}$, determined from a Gaussian fitted to the cross-meridional intensity profile) doubled from rest to the tetanus plateau (Fig. 2*B* and Table 1*A*), with a half-time of $26.8 \pm 4.2$ ms (Table 1*B*). $I_{M3}$ was corrected for the reduction in interfilament coherence by multiplying by the width (Huxley *et al.* 1982). The corrected value ($I_{M3c}$, Fig. 2*C*) was 40% larger at the tetanus plateau than at rest (Table 1*A*). Delaying the initial force rise by imposing unloaded shortening had little effect on the uncorrected $I_{M3}$ (Fig. 2*A*, open circles), but increased the half-time for the $w_{M3}$ change to $40.0 \pm 4.2$ ms (Fig. 2*B* and Table 1*B*). Unloaded shortening also appeared to delay the increase in $I_{M3c}$ (Fig. 2*C*), within the limit of the signal to noise ratio of these measurements.

When unloaded shortening was imposed at the tetanus plateau (Fig. 2*A*, filled circles at times $> 200$ ms), $I_{M3}$ reduced abruptly to almost zero in synchrony with the drop in force. During the 20 ms of unloaded shortening, $I_{M3}$ showed a small progressive recovery to about 20% of its plateau value (Piazzesi *et al.* 1999) (Table 1*A*). Force redevelopment after the end of shortening was accompanied by recovery of $I_{M3}$. It was not possible to measure changes in the radial width of the M3 reflection during unloaded shortening because of its low intensity. However, based on previous work (Huxley *et al.* 1983), the width does not change significantly during rapid shortening imposed at the tetanus plateau. Consequently the $I_{M3}$ changes observed in these conditions are mainly attributable to changes in the number and axial density projection of attached myosin heads.

In the same experiments, the intensity of the M6 reflection ($I_{M6}$) showed a monotonic decrease to 0.25 its resting value during the first half of the rise of the isometric tetanus (Fig. 2*D*, filled circles). The width of the M6 reflection increased to 2.5 times its resting value during the tetanus rise (Table 1*A*). After correction for the width change, $I_{M6}$ at the tetanus plateau was only 10% less than at rest (Table 1*A*). The low signal to noise ratio of the M6 reflection in these experiments prevented a reliable determination of the time course of the width of M6 reflection, or of the corrected $I_{M6}$. The uncorrected $I_{M6}$ data appeared not to be affected by unloaded shortening, either at the start of stimulation (Fig. 2*D*, open circles),

or at the tetanus plateau (Fig. 2*D*, filled circles at times $> 200$ ms and Table 1*A*).

**Spacings of the M3 and M6 reflections.** $S_{M3}$ and $S_{M6}$ increased by ∼1.5% from rest to the tetanus plateau (Table 1*A*; see also Huxley *et al.* 1982; Bordas *et al.* 1993; Linari *et al.* 2000). $S_{M3}$ decreased slightly during the first 5–10 ms after the first stimulus in the isometric tetanus (Fig. 3*A* and *C*, filled circles; see also Piazzesi *et al.* 1999), then started to increase, attaining the tetanus plateau value with a half-time of $31.3 \pm 1.6$ ms (Table 1*B*). Thus the increase of $S_{M3}$ leads that of isometric force by ∼10 ms. Unloaded shortening had no detectable effect on $S_{M3}$ (Fig. 3*A* and *C*, open circles) up to the time corresponding to the end of the isometric latent period ($t_s$). At this time, $S_{M3}$ was slightly smaller than at rest. $S_{M3}$ continued to decrease during $V_0$ shortening after $t_s$ to a minimum of 14.30 nm. Following the end of shortening, $S_{M3}$ increased with a time course parallel to that of $S_{M3}$ in an isometric tetanus, but delayed by ∼10 ms (half-time, $42.2 \pm 1.4$ ms). Thus the increase in $S_{M3}$ in these conditions leads the increase in force by ∼13 ms (Table 1*B*). During the step and ramp shortening imposed at the tetanus plateau, $S_{M3}$ (Fig. 3*A*, filled circles at times $> 200$ ms) decreased progressively from its plateau value (14.56 nm) to a minimum of 14.48 nm at the end of shortening (see also Piazzesi *et al.* 1999) and then recovered to the plateau value as tension redeveloped.

In an isometric tetanus, $S_{M6}$ (Fig. 3*B* and *D*, filled circles) started to increase at the end of the latent period, slightly earlier than $S_{M3}$, and attained its plateau value before $S_{M3}$. The half-time of the increase in $S_{M6}$ was $20.0 \pm 3.5$ ms (Fig. 3*D* and Table 1*B*), which is less than that of force and $S_{M3}$ by ∼20 ms and ∼10 ms, respectively. Initial shortening at $V_0$ did not produce a decrease in $S_{M6}$ below its resting value (Fig. 3*B* and *D*, open circles), only a delayed increase, which started before the end of shortening. The half-time for $S_{M6}$ increased to $32.3 \pm 3.5$ ms, which is ∼12 ms larger than the corresponding value in an isometric tetanus (Table 1*B*). To test whether the low signal to noise ratio affects the estimates of $S_{M6}$ time courses, the analysis was repeated after two-point smoothing. The estimates of half-times for $S_{M3}$ and $S_{M6}$ after smoothing were practically identical to those without smoothing (Table 1*B*). Unloaded shortening at the tetanus plateau appears to produce a slow reduction of $S_{M6}$ (Fig. 3*B*, filled circles at times $> 200$ ms, and Table 1*A*), but the significance of this effect is uncertain due to the low signal to noise ratio.

Comparison of the spacing changes in the M3 and M6 reflections during the tetanus rise shows two main differences. First, the increase of $S_{M6}$ leads that of $S_{M3}$ by ∼10 ms (Table 1*B*), and this lead is maintained when the rise of force is delayed by imposing shortening at $V_0$ just before the end of the latent period. Second, shortening at $V_0$ induces a small (0.24%) but significant reduction in $S_{M3}$ (Fig. 3*C*), but only slows the increase in $S_{M6}$ (Fig. 3*D*). However, the signal to noise ratio of the M6 data collected with RAPID is too low to exclude $S_{M6}$ changes smaller than about 0.25% (Fig. 3*B* and *D*). We therefore repeated the experiments using the FReLoN CCD detector, and in this case the signal to noise ratio was sufficient for the fibres used to be analysed individually (Fig. 4 and Table 2*A* and *B*). In these fibres, $t_s$ was $10.3 \pm 0.3$ ms (mean ± S.D., $n = 3$ fibres) and the half-time for the force rise in the isometric tetanus was $47.0 \pm 1.8$ ms (Table 2*B*), ∼5 ms larger than in the fibres used in the experiments with the RAPID detector (Table 1*B*). The half-time for $S_{M3}$, but not that for $S_{M6}$, increased accordingly. Consequently the lead of the increase of $S_{M6}$ (Fig. 4*A*, open circles) over that of $S_{M3}$ (Fig. 4*A*, filled circles) increased to ∼15 ms (Table 2*B*). Each time course was delayed by ∼10 ms when unloaded shortening was applied soon after the first stimulus (Fig. 4*B* and Table 2*B*). In agreement with the results of the RAPID experiments, shortening at $V_0$ delayed the increase in $S_{M6}$ that started before the end of shortening (Fig. 4*B*, open circles). The reduction of $S_{M3}$ during shortening at $V_0$ (Fig. 4*B*, filled circles) was smaller than in the RAPID

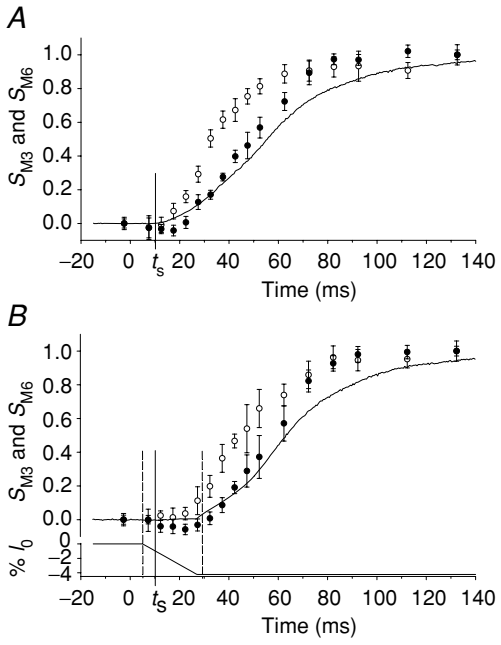


**Figure 4. Effect of unloaded shortening on the time course of $S_{M3}$ and $S_{M6}$ changes during the tetanus rise**
X-ray patterns collected with FReLoN detector. Fractional spacing changes (mean ± S.D. from $n = 3$ fibres) between rest and tetanus plateau. In both *A* and *B* the continuous line is the force. Zero time is the start of stimulation. The vertical continuous lines indicate $t_s$. *A*, $S_{M3}$ (●) and $S_{M6}$ (○) during the rise of the isometric tetanus. *B*, $S_{M3}$ (●) and $S_{M6}$ (○) in tetani with $V_0$ shortening imposed 5 ms after the start of stimulation. Traces are force (upper) and imposed length change (lower). Vertical dashed lines mark the boundary of the average duration of unloaded shortening.

**Table 2. Mechanical and structural parameters collected in experiments with FReLoN detector**

| *A* FReLoN | Rest | $T_0$ | $V_{0,start}$ |
|---|---|---|---|
| $S_{M3}$ (nm) | 14.340 ± 0.004 | 14.561 ± 0.001 | 14.333 ± 0.007 |
| $S_{M6}$ (nm) | 7.157 ± 0.003 | 7.284 ± 0.004 | 7.170 ± 0.010 |
| *B* FReLoN | $t_{1/2,force}$ (ms) | $t_{1/2,SM3}$ (ms) | $t_{1/2,SM6}$ (ms) |
| Isometric | 47.0 ± 1.8 | 37.3 ± 1.1 | 21.7 ± 1.1 |
| $V_{0,start}$ | 55.2 ± 2.4 | 46.4 ± 1.1 | 32.6 ± 1.3 |

*A*, spacing of M3 and M6 reflections at rest, at the isometric tetanus plateau ($T_0$) and during steady shortening at $V_0$ imposed 5 ms after the start of stimulation ($V_{0,start}$). Means ± S.D. from $n = 3$ fibres. The $V_{0,start}$ value is the mean of the last two frames before the end of shortening. $V_0$ in these fibres was 2.16 ± 0.06 $\mu$m s$^{-1}$ (half-sarcomere)$^{-1}$. *B*, half-times of changes of force ($t_{1/2,force}$), spacing of M3 ($t_{1/2,SM3}$) and spacing of M6 ($t_{1/2,SM6}$) in the isometric tetanus (first row) and in the tetanus with shortening at $V_0$ imposed 5 ms after the start of stimulation (second row). The half-time of force is the mean ± S.D. of $n = 3$ fibres. The error for spacing is provided by the sigmoid fitting program.

experiments (Fig. 3*A* and *C*, open circles), and was only detectable in individual fibres if the data for the time frames corresponding to initial shortening at $V_0$ were collected near the start of the series of tetani used to describe the rising phase of the tetanus (see Methods).

### Mechanical and structural changes at the onset of contraction

The mechanical and structural changes at the onset of tetani with and without shortening at $V_0$ are compared in Fig. 5 (thin and thick traces, respectively). The mechanical signals (Fig. 5*A–D*) are from a single fibre with latent period ($t_s$, 10 ms) slightly shorter than the mean for the set of fibres used for the X-ray measurements (Fig. 5*E–H*). The high gain of the mechanical signals reveals that shortening at $V_0$ applied 5 ms after the start of stimulation (~5 ms before $t_s$) generates a small compressive force (~0.005 $T_0$; marked with an asterisk in Fig. 5*D*) that vanishes at $t_s$ (see also Lombardi & Menchetti, 1984). This transient compressive force is due to a resting viscosity that disappears abruptly at the end of the latent period (Ford *et al.* 1977; Lombardi & Menchetti, 1984). In these fibres $T_0$ was 230 ± 26 kPa and $V_0$ was 1.65 ± 0.3 $\mu$m s$^{-1}$ (half-sarcomere)$^{-1}$, so the viscous coefficient is 1.15 kPa/(1650 nm s$^{-1}$ (half-sarcomere)$^{-1}$) = 7 × 10$^8$ N s m$^{-3}$, similar to values reported for a large range of velocities (Ford *et al.* 1977; Lombardi & Menchetti, 1984). This resistance to shortening also appears in the sarcomere length trace as a period of slower shortening (marked with an asterisk in Fig. 5*B*) up to $t_s$, when the sarcomere length change accelerates to the subsequent steady velocity corresponding to that imposed on the fibre (Fig. 5*A*). The difference between the sarcomere length change and fibre length change (Fig. 5*C*) represents the change in extension of the series elasticity due to the tendon attachments, and shows a small transient shortening as expected. During the first 5 ms of shortening when the resting viscosity is present, there is no evident effect of the shortening on either $S_{M3}$ (Fig. 5*E*, from RAPID; Fig. 5*G*, from FReLoN) or $S_{M6}$ (Fig. 5*F*, from RAPID; Fig. 5*H*, from FReLoN); the data from tetani with and without imposed shortening (in Fig. 5 *E–H*, open and filled circles, respectively) are identical within the signal to noise ratio. Therefore it is only after $t_s$ (in Fig. 5 *E–H*, continuous vertical line), when the viscous response disappears, that filament sliding at $V_0$, preventing the force rise, influences the time courses of both meridional reflections. In fact the increase of $S_{M6}$, that starts just after the end of the latent period in isometric contraction (Fig. 5*H*, filled circles), is only delayed by shortening at $V_0$ (Fig. 5*H*, open circles), so that at the end of shortening, 29 ms after the start of stimulation, $S_{M6}$ is 7.17 nm (Table 2*A*), 0.3% smaller than in the corresponding time frame in an isometric tetanus, but 0.2% larger than at rest. In contrast, $S_{M3}$ does not increase or slightly decreases for the first 10 ms following the latent period (the first two frames after $t_s$) in isometric contraction (Fig. 5*E* and *G*, filled circles), and further decreases in tetani with shortening at $V_0$ (Fig. 5*E* and *G*, open circles), so that at the end of shortening it is 14.31 nm in the experiments with RAPID (Fig. 5*E* and Table 1*A*) and 14.33 nm in those with FReLoN (Fig. 5*G* and Table 2*A*), smaller than the resting value by 0.2% and 0.07%, respectively.

### The effects of delaying the isometric force development at 0.5 $T_0$

In two experiments, isometric force development was interrupted at ~65 ms after the start of stimulation, when the force was 0.5 $T_0$, by applying a ramp shortening at a velocity ~$^1/_4$ $V_0$ or 0.4 $\mu$m s$^{-1}$ (half-sarcomere)$^{-1}$ (Fig. 6, thin lines and open circles). To compare the results with those obtained for the same force and shortening velocity at full activation, the shortening ramp was also imposed at the tetanus plateau, 235 ms after the start of stimulation (Fig. 6, thick lines and filled circles after 200 ms). In this case, the ramp shortening was preceded by a step release of 4–5 nm (half-sarcomere)$^{-1}$ to accelerate the drop of force to 0.5 $T_0$.

Imposition of steady shortening to interrupt the rise of force at 0.5 $T_0$ led to a further decrease in $I_{M3}$ (Fig. 6*A*, open circles), in contrast with the increase in $I_{M3}$ in this period of an isometric tetanus (Figs 2*A* and 6*A*, filled circles). Following the end of shortening, $I_{M3}$ started to recover

towards its value at the tetanus plateau. When shortening at $\sim$1/4 $V_0$ was imposed at the tetanus plateau, $I_{M3}$ dropped suddenly to a value similar to that maintained during shortening at 1/4 $V_0$ during the tetanus rise (Table 3). Changes in the radial width of the reflection were not taken into account in this analysis because the signal to noise ratio of the width for two fibres was too low. However the half-time for $w_{M3}$ in isometric conditions is 27 ms (Fig. 2), and little further change is expected after 65 ms, when shortening at 1/4 $V_0$ was imposed. The data in Fig. 6*A* show that the reduction of $I_{M3}$ produced by shortening at 1/4 $V_0$ does not depend on the phase of the tetanus, but only on the sliding velocity and the force.

In contrast with the behaviour of $I_{M3}$, $S_{M3}$ was not affected by shortening at 1/4 $V_0$. $S_{M3}$ continued to increase from its value of 14.45 nm at 65 ms after the start of stimulation to its value at the tetanus plateau with the same time course as in an isometric tetanus (Fig. 6*B*). Moreover, $S_{M3}$ was also not affected by shortening at 1/4 $V_0$ applied at the tetanus plateau (Fig. 6*B* and Table 3).

Changes in the M6 reflection could not be measured with adequate signal to noise ratio in single time frames in these two fibres, but it was possible to measure $I_{M6}$ and $S_{M6}$ at the tetanus plateau and during the second part of shortening at 1/4 $V_0$ imposed either during the tetanus rise or at the plateau, by adding data from 10 to 16 frames. $I_{M6}$ was $\sim$50% higher during shortening at 1/4 $V_0$, compared to its plateau value and $S_{M6}$ remained constant (Table 3).

## Discussion

### Kinetics of isometric force generation

The strain of the half-sarcomere during the rise of the isometric tetanus, calculated from stiffness measurements

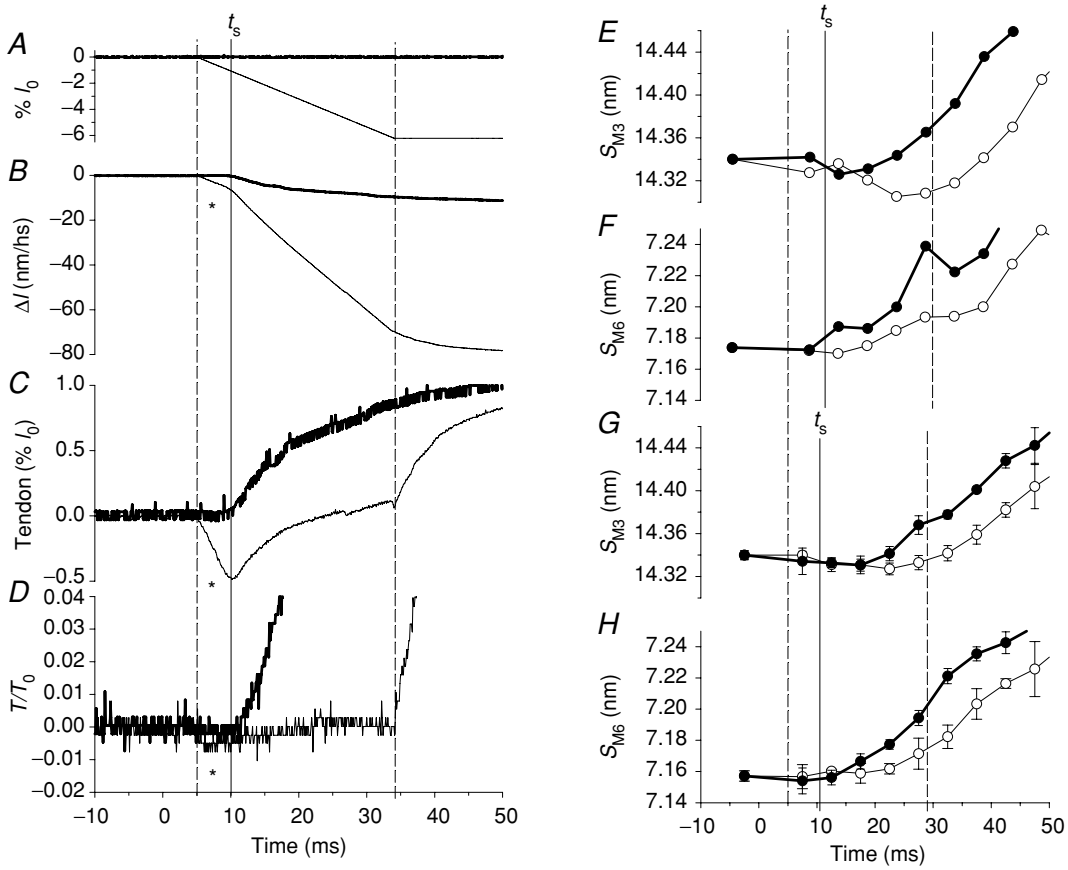


**Figure 5. Mechanical and structural signals at the onset of contraction**
In all the frames the vertical continuous line marks $t_s$, the dashed lines mark the boundary of the period of unloaded shortening. *A–D*, thick line, isometric condition; thin line, unloaded shortening imposed 5 ms after the start of stimulation. *A*, fibre length change imposed by the motor; shortening in % $l_0$, where $l_0$ is the fibre length. *B*, length change in nm per half-sarcomere ($\Delta l$) measured in the selected fibre segment. Note that during the first 5 ms of imposed shortening (denoted by *), the half-sarcomere shortens at a velocity lower than $V_0$; $V_0$ shortening starts 10 ms after the first stimulus, at the end of the latent period, when in the isometric contraction the half-sarcomere starts to shorten against the end compliance. *C*, difference between fibre length change in *A* and half-sarcomere length change in *B*, both expressed in % $l_0$ (where $l_0$ for *B* is the half-sarcomere length). *D*, force. *E* and *F*, $S_{M3}$ and $S_{M6}$ from RAPID experiments in isometric conditions (●) and during the imposed $V_0$ shortening (○). *G* and *H*, $S_{M3}$ and $S_{M6}$ from FReLoN experiments. Same symbols as in *E* and *F*.

made with 4 kHz sinusoidal length oscillations, has been found to increase with the isometric force (Fig. 1*D*). Taking into account the contribution of actin and myosin filaments to the half-sarcomere strain, we showed that the average strain in the attached myosin heads, 1.8 nm, remains constant in the range of isometric forces investigated (from $0.25\,T_0$ to $T_0$), indicating that the increase in force is proportional to the increase in the number of myosin heads attached to actin.

Force generation at the molecular level is therefore due to a rapid equilibrium between different force generating states of the attached myosin head, as proposed in the mechanical–kinetic model of Huxley & Simmons (1971), and the rate of force generation in an isometric tetanus is limited by the rate of attachment of myosin heads to actin.

Mechanical (Piazzesi *et al.* 2003; Decostre *et al.* 2005) and structural (Lombardi *et al.* 1995; Dobbie *et al.* 1998; Irving *et al.* 2000) studies on muscle fibres have produced compelling evidence that the average conformation of attached myosin heads in an isometric tetanus is near the beginning of their working stroke. This is also consistent with the consideration that the average strain in the myosin heads in isometric contraction (1.8 nm; Fig. 1) is one order of magnitude smaller than the axial displacement of the heads during the working stroke (12 nm, Ford *et al.* 1977; Reconditi *et al.* 2004).

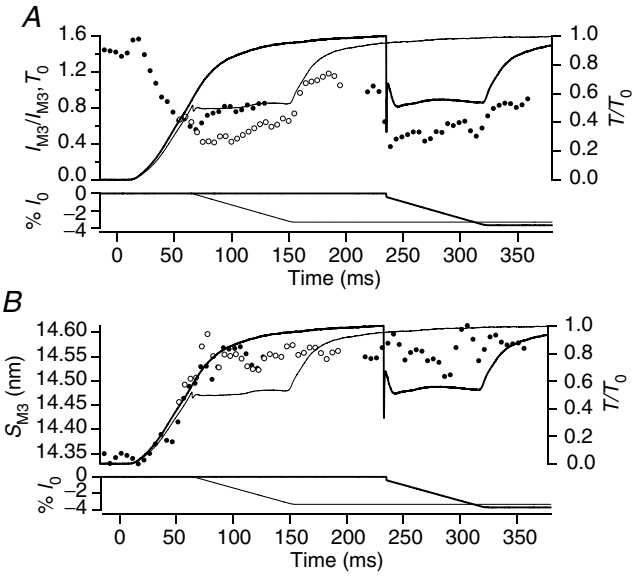


**Figure 6. Effect of shortening at ¼ $V_0$ on $I_{M3}$ (*A*) and $S_{M3}$ (*B*)**
Filled circles, X-ray data collected in tetani with ¼ $V_0$ shortening imposed at the isometric plateau (thick lines); open circles, X-ray data collected in tetani with ¼ $V_0$ shortening imposed 65 ms after the start of stimulation (thin lines). Data collected on the RAPID detector. In each panel lower traces are the imposed length changes (% $l_0$) and upper traces the corresponding force responses (relative to $T_0$).

**Table 3. Intensity and spacing of M3 and M6 reflections in experiments with shortening at ¼ $V_0$**

| RAPID | Rest | $T_0$ | ¼ $V_{0,\mathrm{start}}$ | ¼ $V_{0,T0}$ |
|---|---|---|---|---|
| $S_{M3}$ (nm) | 14.34 | 14.54 | 14.52 | 14.55 |
| $S_{M6}$ (nm) | 7.16 | 7.29 | 7.27 | 7.28 |
| $I_{M3}$ | 1.83 | 1 | 0.71 | 0.65 |
| $I_{M6}$ | — | 1 | 1.63 | 1.5 |

Intensity and spacing collected with RAPID detector at rest, at $T_0$ and during steady shortening at ¼ $V_0$ imposed either 65 ms after the start of stimulation (¼ $V_{0,\mathrm{start}}$) or at $T_0$ (¼ $V_{0,T0}$). X-ray data obtained adding X-ray patterns from several time frames from two fibres as explained in the text.

## Structural changes in the myosin filament during the tetanus rise

The spacings of the M3 and M6 reflections ($S_{M3}$ and $S_{M6}$) increase by the same extent (~1.5%) during isometric force development, but with different time courses (Tables 1 and 2; and Figs 3 and 4), supporting the view that the two reflections originate from different components of the myosin filament (Huxley *et al.* 2003). The increase in $S_{M6}$ leads that of $S_{M3}$ by ~10 ms and that of isometric force by ~20 ms. The changes in the intensities of the two reflections during the rising phase of an isometric tetanus provide further evidence for their distinct origins, once they are corrected for the reduction in interfilament coherence associated with force development (Fig. 2). The corrected $I_{M3}$ increased by 40% with respect to its resting value, whereas the corrected $I_{M6}$ showed no significant change (Table 1*A*). The changes in $S_{M3}$ and $I_{M3}$ have been explained as the weighted contributions of two populations of myosin heads, a decaying population (the resting myosin heads) with spacing 14.34 nm, and a rising population (the heads attached to actin) with spacing 14.57 nm (Piazzesi *et al.* 1999). The contribution of the 14.57 nm component of the M3 reflection was found to increase with a time course similar to that of the isometric force (Piazzesi *et al.* 1999). Because, as shown in the previous section, the increase in force is proportional to the increase in the number of myosin heads attached to actin, the 14.57 nm component of the M3 reflection can be identified with the attached myosin heads. The finding that $I_{M6}$ does not change during force development is a further decisive test of the idea that the M6 reflection mainly originates from other periodic structures on the myosin filament (Huxley *et al.* 2003; Reconditi *et al.* 2004).

The half-time of the $S_{M6}$ increase during the tetanus rise (20 ms) is about half of that of the force increase. We previously showed that the half-times of the reduction in the intensities of other myosin-based reflections related to the resting structure of the thick filament were also less

than that of force (Piazzesi *et al.* 1999). The half-time of the decrease in the intensity of the first myosin-based layer line (ML1, at 42 nm), the second myosin-based meridional (M2, at 21 nm) and the 14.34 nm resting component of the M3 reflection were ∼19, 19 and 24 ms, respectively. On the other hand the reflection amplitudes (the square root of the intensity) decreased with time courses closer to that of force, and thus can be considered as an alternative measure of the number of myosin heads with a resting-like conformation. The M6 reflection appears distinct from other X-ray reflections associated with resting or active periodic structures in the myosin filament based on a ∼43 nm axial repeat (for example, myosin binding protein C) in that, unlike the M2 and ML1 reflections, it remains intense during activation. The M6 reflection is much less sensitive than the M3 reflection to mechanical manoeuvres that change the form factor of attached myosin heads (Reconditi *et al.* 2004; Huxley *et al.* 2003; and this work). Thus the M6 reflection originates mainly from a structure with the same axial periodicity as the myosin heads but located in the backbone of the myosin filament. Consequently, the changes in the spacing of the M6 reflection signal changes in the length of the myosin filament during the transition from rest to the tetanus plateau that are unaffected by and precede myosin head attachment.

### Mechanical and structural changes at the onset of contraction

Following depolarization of the cell membrane, a frog muscle fibre develops force with a delay of ∼11 ms at 4°C. Before that time, the only mechanical sign of activation in isometric conditions is a small reduction of resting tension (latency relaxation) that occurs just before the end of the latent period and becomes more evident at sarcomere lengths longer than the 2.15 $\mu$m used in this work (Lannergren, 1971; Haugen & Sten-Knudsen, 1976). The end of the latent period has been shown to coincide with the decrease in the resting viscosity of the fibre (Ford *et al.* 1977; Lombardi & Menchetti, 1984). This resting viscosity was first described as a short-range elastic component and attributed to a small number of cross-bridges attached at rest (Hill, 1968), but its nature is still unclear (Bagni *et al.* 1995; Proske & Morgan, 1999) When shortening at $V_0$ is imposed at rest or during the latent period, this viscosity appears as a small compressive force (∼0.005 $T_0$), corresponding to a viscous coefficient of $7 \times 10^8$ N s m$^{-3}$, and vanishes abruptly at the end of the latent period (Lombardi & Menchetti, 1984). This viscous coefficient is similar to that found by stretching resting fibres at a wide range of velocities (Ford *et al.* 1977; Bagni *et al.* 1998). In the present experiments, as shown in Fig. 5, the phenomenon also appears as a reduction in the velocity of shortening of the sarcomeres (Fig. 5*B*) compared to the velocity imposed at the fibre end (Fig. 5*A*). The transient difference between the imposed velocity and the sarcomere velocity gives the length change of the series elasticity (presumably tendon attachments, Fig. 5*C*) that shortens in correspondence to the compressive force.

Within 10 ms after the end of the latent period, $S_{M6}$ has already started to increase during an isometric tetanus, whereas $S_{M3}$ has not changed or is slightly reduced. The different origin of the M3 and M6 reflections is further shown by imposing shortening at $V_0$ to delay force development: the increase in $S_{M6}$ is slowed but not prevented by shortening, whereas $S_{M3}$ decreases further. When data were collected using different time frames in a series of tetani (FReLoN detector), the decrease was less marked than when the whole series of time frames was collected in each tetanus (RAPID detector), suggesting that the $S_{M3}$ decrease is larger in fresh fibres. The origin of this vulnerability to repeated stimulation or X-ray exposure is unknown, but it is clear that $S_{M3}$ but not $S_{M6}$ is sensitive to mechanical perturbation almost immediately after the resting viscosity has disappeared, providing further evidence that the M3 reflection is much more sensitive to the motions of the myosin heads than the M6 reflection. The delayed rise of $I_{M3}$ caused by the imposition of unloaded shortening (Fig. 2*C*) provides yet more evidence for this distinction.

Unloaded shortening imposed at the tetanus plateau induces: (1) a progressive decrease in $S_{M3}$, with much less change in $S_{M6}$ and (2) an abrupt reduction of $I_{M3}$, without effect on $I_{M6}$. The reduction of $I_{M3}$ is explained by the tilting of the light-chain domains of the myosin heads towards the end of the working stroke (Irving *et al.* 2000; Reconditi *et al.* 2004), again suggesting that this reflection originates from the attached myosin heads.

In active muscle $S_{M6}$ depends linearly on the force independently of the method (length or force steps, temperature change) used to modulate the force, or the speed of the force change. The compliance of the myosin filament determined from this unique stress–strain relation is 0.26%/$T_0$ (Piazzesi *et al.* 2002; Reconditi *et al.* 2004; Linari *et al.* 2005). In contrast, the same experiments showed that the relation between $S_{M3}$ and force is not unique, because $S_{M3}$ is influenced by the method and the speed of force modulation, and thus by the distribution and conformation of myosin heads attached to actin.

Steady shortening at $^1/_4$ $V_0$ reduces the force to 0.5 $T_0$, according to the force–velocity relation. In these conditions the distribution of tilting of the attached myosin heads should be shifted in agreement with the progression in the working stroke, and the number of attached heads should be reduced (Huxley, 1957; Ford *et al.* 1985; Piazzesi & Lombardi, 1995). These factors would be expected to reduce the intensity of X-ray reflections originating from attached myosin heads, as observed for the M3 reflection

(Table 3). The same $I_{M3}$ reduction occurs at the tetanus plateau, when the force drops from $T_0$ to 0.5 $T_0$, and during the tetanus rise, when the isometric force is prevented from increasing beyond 0.5 $T_0$.

Holding the force at 0.5 $T_0$ during the tetanus rise does not prevent the attainment of the plateau value of $S_{M3}$ (Fig. 6*B*, open circles), just as decreasing the plateau force to 0.5 $T_0$ does not reduce $S_{M3}$ (Fig. 6*B*, filled circles). $S_{M6}$ is likewise unaffected by the decrease of steady force from $T_0$ to 0.5 $T_0$ (Table 3). These results refer to the large spacing changes of the type observed during the rise of the tetanus and during shortening at $V_0$. The much smaller spacing changes related to the elasticity of the myosin filament ($\sim$0.26%/$T_0$, Reconditi *et al.* 2004) are likely to be present when force is modulated by shortening, but would not be resolved with the signal to noise ratio of the data shown in Fig. 6 and Table 3. In conclusion, both the M3 and M6 reflections maintain the spacing characteristic of active isometric contraction even during shortening that maintains the force $\geq 0.5\,T_0$. Only shortening at $V_0$ induces a partial recovery towards the resting spacing (Piazzesi *et al.* 1999).

The idea that the myofilaments and myosin heads are already fully activated at the halfway point of the tetanus rise was first put forward on the basis that the force–velocity relation attains its steady-state characteristics before the isometric force (Cecchi *et al.* 1978). The evidence from the present work that both the intensity and the spacing of the M3 and M6 reflections respond to shortening in the same way at the halfway point of the tetanus rise as at the plateau gives structural support to this proposal. However, only the intensity of the M3 reflection is sensitive to changes in the number and axial density projection of the myosin heads. Upon activation, the myosin filament structure generating the M6 reflection undergoes the same 1.5% increase in periodicity as the myosin head-based M3 reflection. However the findings that: (1) $I_{M6}$ does not change during the tetanus rise, (2) the increase of $S_{M6}$ precedes that of $S_{M3}$ and force, and (3) both $I_{M6}$ and $S_{M6}$ show a reduced sensitivity to mechanical manoeuvres, support the view that the M6 reflection mainly arises from another component of the myosin filament, and that the myosin heads make only a small contribution to this reflection.

## References


Bagni MA, Cecchi G, Cecchini E, Colombini B & Colomo F (1998). Force responses to fast ramp stretches in stimulated frog skeletal muscle fibres. *J Muscle Res Cell Motil* **19**, 33–42.

Bagni MA, Cecchi G, Colomo F & Garzella P (1995). Absence of mechanical evidence for attached weakly binding cross-bridges in frog relaxed muscle fibres. *J Physiol* **482**, 391–400.

Bordas J, Diakun GP, Diaz FG, Harries JE, Lewis RA, Lowy J, Mant GR, Martin-Fernandez ML & Towns-Andrews E (1993). Two-dimensional time-resolved X-ray diffraction studies of live isometrically contracting frog sartorius muscle. *J Muscle Res Cell Motil* **14**, 311–324.

Cecchi G, Colomo F & Lombardi V (1978). Force-velocity relation in normal and nitrate-treated frog single muscle fibres during rise of tension in an isometric tetanus. *J Physiol* **285**, 257–273.

Cecchi G, Colomo F, Lombardi V & Piazzesi G (1987). Stiffness of frog muscle fibres during rise of tension and relaxation in fixed-end or length-clamped tetani. *Pflugers Arch* **409**, 39–46.

Cecchi G, Griffiths PJ, Bagni MA, Ashley CC & Maeda Y (1991). Time-resolved changes in equatorial x-ray diffraction and stiffness during rise of tetanic tension in intact length-clamped single muscle fibers. *Biophys J* **59**, 1273–1283.

Cecchi G, Griffiths PJ & Taylor S (1982). Muscular contraction: kinetics of crossbridge attachment studied by high-frequency stiffness measurements. *Science* **217**, 70–72.

Decostre V, Bianco P, Lombardi V & Piazzesi G (2005). Effect of temperature on the working stroke of muscle myosin. *Proc Natl Acad Sci U S A* **102**, 13927–13932.

Dobbie I, Linari M, Piazzesi G, Reconditi M, Koubassova N, Ferenczi MA, Lombardi V & Irving M (1998). Elastic bending and active tilting of myosin heads during muscle contraction. *Nature* **396**, 383–387.

Ford LE, Huxley AF & Simmons RM (1977). Tension responses to sudden length change in stimulated frog muscle fibres near slack length. *J Physiol* **269**, 441–515.

Ford LE, Huxley AF & Simmons RM (1985). Tension transients during steady shortening of frog muscle fibres. *J Physiol* **361**, 131–150.

Ford LE, Huxley AF & Simmons RM (1986). Tension transients during the rise of tetanic tension in frog muscle fibres. *J Physiol* **372**, 595–609.

Haselgrove JC (1975). X-ray evidence for conformational changes in the myosin filaments of vertebrate striated muscle. *J Mol Biol* **92**, 113–143.

Haselgrove JC & Huxley HE (1973). X-ray evidence for radial cross-bridge movement and for the sliding filament model in actively contracting skeletal muscle. *J Mol Biol* **77**, 549–568.

Haugen P & Sten-Knudsen O (1976). Sarcomere lengthening and tension drop in the latent period of isolated frog skeletal muscle fibers. *J Gen Physiol* **68**, 247–265.

Hill DK (1968). Tension due to interaction between the sliding filaments in resting striated muscle. The effect of stimulation. *J Physiol* **199**, 637–684.

Huxley AF (1957). Muscle structure and theories of contraction. *Prog Biophys Biophys Chem* **7**, 255–318.

Huxley AF & Lombardi V (1980). A sensitive force transducer with resonant frequency 50 kHz. *J Physiol* **305**, 15–16*P*.

Huxley AF, Lombardi V & Peachey LD (1981). A system for fast recording of longitudinal displacement of a striated muscle fibre. *J Physiol* **317**, 12–13*P*.

Huxley AF & Simmons RM (1971). Proposed mechanism of force generation in striated muscle. *Nature* **233**, 533–538.

Huxley HE & Brown W (1967). The low-angle x-ray diagram of vertebrate striated muscle and its behaviour during contraction and rigor. *J Mol Biol* **30**, 383–434.

Huxley HE, Faruqi AR, Kress M, Bordas J & Koch MH (1982). Time-resolved X-ray diffraction studies of the myosin layer-line reflections during muscle contraction. *J Mol Biol* **158**, 637–684.

Huxley HE, Reconditi M, Stewart A & Irving T (2003). What the higher order meridional reflections tell us. *Biophys J* **84**, 139a.

Huxley HE, Simmons RM, Faruqi AR, Kress M, Bordas J & Koch MH (1983). Changes in the X-ray reflections from contracting muscle during rapid mechanical transients and their structural implications. *J Mol Biol* **169**, 469–506.

Huxley HE, Stewart A, Sosa H & Irving T (1994). X-ray diffraction measurements of the extensibility of actin and myosin filaments in contracting muscle. *Biophys J* **67**, 2411–2421.

Irving M, Piazzesi G, Lucii L, Sun Y-B, Harford JJ, Dobbie IM, Ferenczi MA, Reconditi M & Lombardi V (2000). Conformation of the myosin motor during force generation in skeletal muscle. *Nat Struct Biol* **7**, 482–485.

Juanhuix J, Bordas J, Campmany J, Svensson A, Bassford ML & Narayanan T (2001). Axial disposition of myosin heads in isometrically contracting muscles. *Biophys J* **80**, 1429–1441.

Lannergren J (1971). The effect of low-level activation on the mechanical properties of isolated frog muscle fibers. *J Gen Physiol* **58**, 145–162.

Lewis RA, Fore NS, Helsby WI, Hall C, Jones A, Parker B, Sumner I, Worgan JS & Budtz-Jørgensen C (1992). High counting rate gaseous X-ray detectors for synchrotron radiation applications. *Rev Sci Instrum* **63**, 642–647.

Linari M, Brunello E, Reconditi M, Sun Y-B, Panine P, Narayanan T, Piazzesi G, Lombardi V & Irving M (2005). The structural basis of the increase in isometric force production with temperature in frog skeletal muscle. *J Physiol* **567**, 459–469.

Linari M, Piazzesi G, Dobbie I, Koubassova N, Reconditi M, Narayanan T, Diat O, Irving M & Lombardi V (2000). Interference fine structure and sarcomere length dependence of the axial X-ray pattern from active single muscle fibers. *Proc Natl Acad Sci U S A* **97**, 7226–7231.

Lombardi V & Menchetti G (1984). The maximum velocity of shortening during the early phases of the contraction in frog single muscle fibres. *J Muscle Res Cell Motil* **5**, 503–513.

Lombardi V & Piazzesi G (1990). The contractile response during steady lengthening of stimulated frog muscle fibres. *J Physiol* **431**, 141–171.

Lombardi V, Piazzesi G, Ferenczi MA, Thirlwell H, Dobbie I & Irving M (1995). Elastic distortion of myosin heads and repriming of the working stroke in muscle. *Nature* **374**, 553–555.

Martin-Fernandez ML, Bordas J, Diakun G, Harries J, Lowy J, Mant GR, Svensson A & Towns-Andrews E (1994). Time-resolved X-ray diffraction studies of myosin head movements in live frog sartorius muscle during isometric and isotonic contractions. *J Muscle Res Cell Motil* **15**, 319–348.

Narayanan T, Diat O & Boesecke P (2001). SAXS and USAXS on the high brilliance beamline at the ESRF. *Nucl Instrum Methods Phys Res A* **467**, 1005–1009.

Piazzesi G & Lombardi V (1995). A cross-bridge model that is able to explain mechanical and energetic properties of shortening muscle. *Biophys J* **68**, 1966–1979.

Piazzesi G, Reconditi M, Dobbie I, Linari M, Boesecke P, Diat O, Irving M & Lombardi V (1999). Changes in conformation of myosin heads during the development of isometric contraction and rapid shortening in single frog muscle fibres. *J Physiol* **514**, 305–312.

Piazzesi G, Reconditi M, Koubassova N, Decostre V, Linari M, Lucii L & Lombardi V (2003). Temperature dependence of the force-generating process in single fibres from frog skeletal muscle. *J Physiol* **549**, 93–106.

Piazzesi G, Reconditi M, Linari M, Lucii L, Sun Y-B, Narayanan T, Boesecke P, Lombardi V & Irving M (2002). Mechanism of force generation by myosin heads in skeletal muscle. *Nature* **415**, 659–662.

Proske U & Morgan DL (1999). Do cross-bridges contribute to the tension during stretch of passive muscle? *J Muscle Res Cell Motil* **20**, 433–442.

Reconditi M, Linari M, Lucii L, Stewart A, Sun Y-B, Boesecke P, Narayanan T, Fischetti RF, Irving T, Piazzesi G, Irving M & Lombardi V (2004). The myosin motor in muscle generates a smaller and slower working stroke at higher load. *Nature* **428**, 578–581.

Wakabayashi K, Sugimoto Y, Tanaka H, Ueno Y, Takezawa Y & Amemiya Y (1994). X-ray diffraction evidence for the extensibility of actin and myosin filaments during muscle contraction. *Biophys J* **67**, 2422–2435.

## Acknowledgements

We thank A. Aiazzi, M. Dolfi and J. Gorini for mechanical and electronics support. This work was supported by Ministero dell'Istruzione, dell'Università e della Ricerca (Italy), Medical Research Council (UK), European Molecular Biology Laboratory and European Synchrotron Radiation Facility. E.B. was supported by a PhD fellowship from Istituto Nazionale di Fisica della Materia (Italy).